ACS APPLIED MATERIALS & INTERFACES

www.acsami.org Research Article

A High-Performance Flexible Pressure Sensor Realized by Overhanging Cobweb-like Structure on a Micropost Array

Weiguan Zhang, Yan Xiao, Yu Duan, Ning Li, Linlin Wu, Yan Lou, Hao Wang,* and Zhengchun Peng*

Cite This: *ACS Appl. Mater. Interfaces* 2020, 12, 48938–48947 Read Online

ACCESS | Metrics & More | Article Recommendations | Supporting Information

ABSTRACT: Recent years have seen a rapid development of electronic skin for wearable devices, autonomous robotics, and human–machine interaction. As a result, the demand for flexible pressure sensors as the critical sensing element in electronic skin is also increasing. These sensors need to feature high sensitivity, short response time, low detection limit, and so on. In this paper, inspired from the cobweb in nature, we propose a piezoresistive pressure sensor by forming a cobweb-like network made of a zinc octaethylphorphyrin (ZnOEP)/carbon nanotube (CNT) hybrid on an array of polydimethylsiloxane (PDMS) microposts. The hybrid material exhibits excellent adhesion to PDMS, benefitting from ZnOEP's low Young's modulus and the nonpolar bonding between ZnOEP and PDMS such that no delamination and resistance variation are found after thousands of cycles of bending and twisting. With the overhanging morphology of the ZnOEP/CNT network on the micropost array, we realized a pressure sensor with an ultrahigh sensitivity of 39.4 kPa^{-1}, a super-fast response time of 3 ms, a low detection limit of 10 Pa, and a reproducible response without degradation after 5000 cycles of pressure loading/unloading. The sensor can be employed for a variety of applications, including wrist pulse measurement, sound level detection, mechanical vibration monitoring, etc., proving its great potential for use in electronic skin systems.

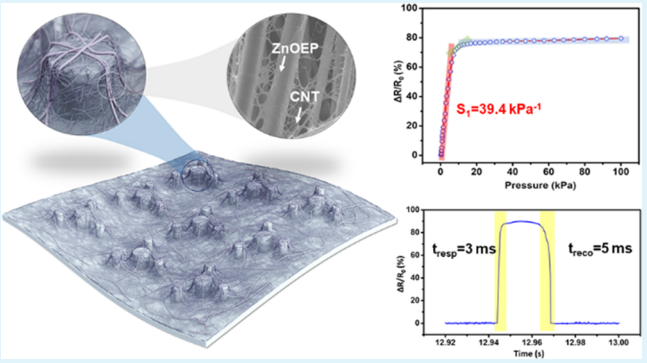

KEYWORDS: *flexible pressure sensor, cobweb-inspired design, overhanging morphology, ZnOEP/CNT hybrid, ultrahigh sensitivity*

1. INTRODUCTION

Flexible pressure sensors that convert physical pressure into electrical signals play an important role in electronic skin for tactile sensing of soft robots,[1] health monitoring,[2] and human–machine interaction.[3] A variety of sensing mechanisms, including piezoresistive,[4−6] piezocapacitive,[7,8] piezoelectric,[9−11] and triboelectric,[12−14] have been proposed for flexible pressure sensors. Among these different sensing mechanisms, piezocapacitive type sandwiches a compressible dielectric material between the two electrodes and converts the external pressure to the change of capacitance. Piezocapacitive sensors demonstrate the merits of high sensitivity, low drift, compatiblity with static measurement, and long-term stability; however, the fringe effect of the capacitor makes the sensor susceptible to the approaching objects and affects the signal accuracy during measurement. Piezoelectric and triboelectric pressure sensors make use of the piezoelectric and triboelectric effects of specific materials (e.g., PVDF, AIN, ZnO, and BaTiO3) that transfer mechanical energy into electrical energy. These sensors are great for transient or dynamic pressure detection, benefitting from their high sensitivity and fast response time, also consuming very little power or do not even need an external power supply due to the energy harvesting property. Piezoresistive pressure sensors take advantage of a piezoresistive effect that transduces the applied pressure into the resistance change of the material. Owing to their simple fabrication, easy signal acquisition, and broad sensing range, piezoresistive pressure sensors have been widely studied.

Generally, a resistive pressure sensor responds to external pressure by a change in the resistance of a conductive layer. For a flexible resistive pressure sensor, this layer is typically produced by dip/spin coating or transferring of conductive materials like carbon allotropes or metal nanowires onto flexible organic substrates. Carbon nanotubes (CNTs),[15,16] graphene,[17,18] silver nanowires (AgNWs),[19,20] or gold nanowires[21,22] are widely used for making these layers owing to their good conductivity or specific morphology that leads to high sensitivity of sensors. Because of the poor adhesion between the organic and inorganic material due to the large Young's modulus mismatch, sensors fabricated by this approach are often subject to the delamination of the piezoresistive layer from the substrate, resulting in the

Received: July 8, 2020
Accepted: September 25, 2020
Published: September 25, 2020

https://dx.doi.org/10.1021/acsami.0c12369
ACS Appl. Mater. Interfaces 2020, 12, 48938–48947

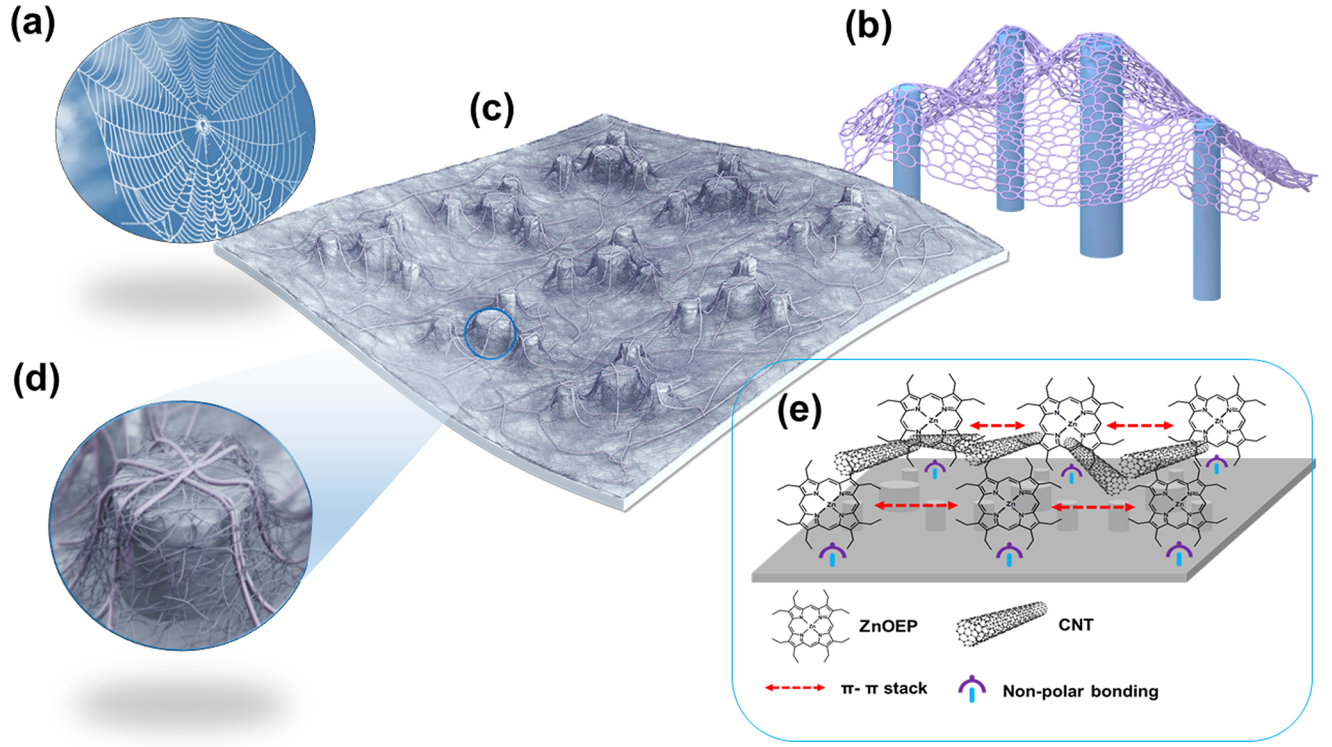

Figure 1. (a) Cobweb in nature. (b) Conception of a 3D cobweb-like structure. (c) Schematic illustration of the cobweb-like hybrid material coated on a micropost array. (d) Enlarged image shows the cobweb-like hybrid material on a micropost where the ZnOEP, which is thicker, formed the scaffold of the cobweb-like structure, and CNTs, which are denser and thinner, formed the networks in between the scaffolds. (e) Molecular structure of the $\pi-\pi$ stacked ZnOEP connected with CNTs and their nonpolar bonding with the PDMS substrate.

failure of the device. To solve this problem, Gaynor et al. proposed a method for fabricating the piezoresistive sensor by embedding AgNWs into a polymer surface,[23] while Lee et al. introduced a poly(diallyldimethlyammonium chloride) (PDDA) buffer layer between the AgNW layer and the substrate to increase the adhesion.[24] Graphene and CNTs have also been used as a protective coating for the AgNW layer to improve their stability.[25,26] In the aforementioned approaches, the materials were mixed physically, which means that the drawbacks of the inorganic materials, such as their unstable mechanical properties, still exist.

Therefore, organic/inorganic hybrids that utilize the merits of both materials are desired.[27] Among the reported organic materials, organic small conjugated molecules, due to their simple fabrication, low modulus, and easy self-assembly, have the advantages in creating a flexible scaffold that is compliant with a flexible substrate.[28] Zinc octaethylphorphyrin (ZnOEP) is one of the most widely used π-conjugated functional organic materials because of its chemical and thermal stability as well as its solubility, which enables easy combination with other materials.[29] Different inorganic materials have been studied to hybridize with organic materials owning to their unique properties. Graphene and CNTs are two kinds of typical carbon-based inorganic materials with the merits of excellent electric properties and great flexibility, both of which lead to their wide use in flexible devices, particularly in a hybridized form with organic materials. The synthesis process of the hybrid material can be achieved through covalent bonding, which is simple and time-saving. Graphene has been reported to improve the optoelectronic properties of the hybrid material,[30] and photovoltaic properties, which are critical for perovskite solar cells, can be enhanced by metal−organic frameworks.[31] Benefitting from CNTs' interlaced networking structure and good conductivity, they are often employed to create conducting paths of the hybrid material,[32] which exhibit great potential for flexible devices.

On the other hand, microstructures have been widely studied to enhance the performance of pressure sensors, specifically sensitivity and linear sensing range. The microstructures could be arrays of regular shapes, such as microdomes, micropyramids, and micropillars,[33−37] created using standard microfabrication processes or replicated from natural templates such as lotus leaves, fingerprints, skin, and sandpaper.[38−41] Generating a thin layer of a piezoresistive material on the microstructures can further improve the sensitivity of the pressure sensors as the piezoresistive material becomes more deformable with the microstructures. Nevertheless, most of these microstructures typically feature a slope to enable conformal adhesion of the piezoresistive materials to them. As such, the change in resistance due to external pressure is fully determined by the deformation of the microstructures. Suspending the piezoresistive material on a microstructure in a 3D cobweb-like structure allows more deformation before they fully attach to the substrate, which should lead to higher sensitivity to the applied pressure.

In nature, a cobweb is highly flexible and tenacious, which could firmly capture insects on it (Figure 1a). Inspired from the cobweb in nature, we believe that such a 3D overhanging structure design can enhance the performance of flexible piezoresistive pressure sensors. For the first time, we realized a cobweb-like network by self-assembling CNTs among a ZnOEP scaffold in this study. To further optimize the sensor performance, we creatively turned the 2D network into a 3D overhanging cobweb-like structure (Figure 1b) by forming the

https://dx.doi.org/10.1021/acsami.0c12369
ACS Appl. Mater. Interfaces 2020, 12, 48938−48947

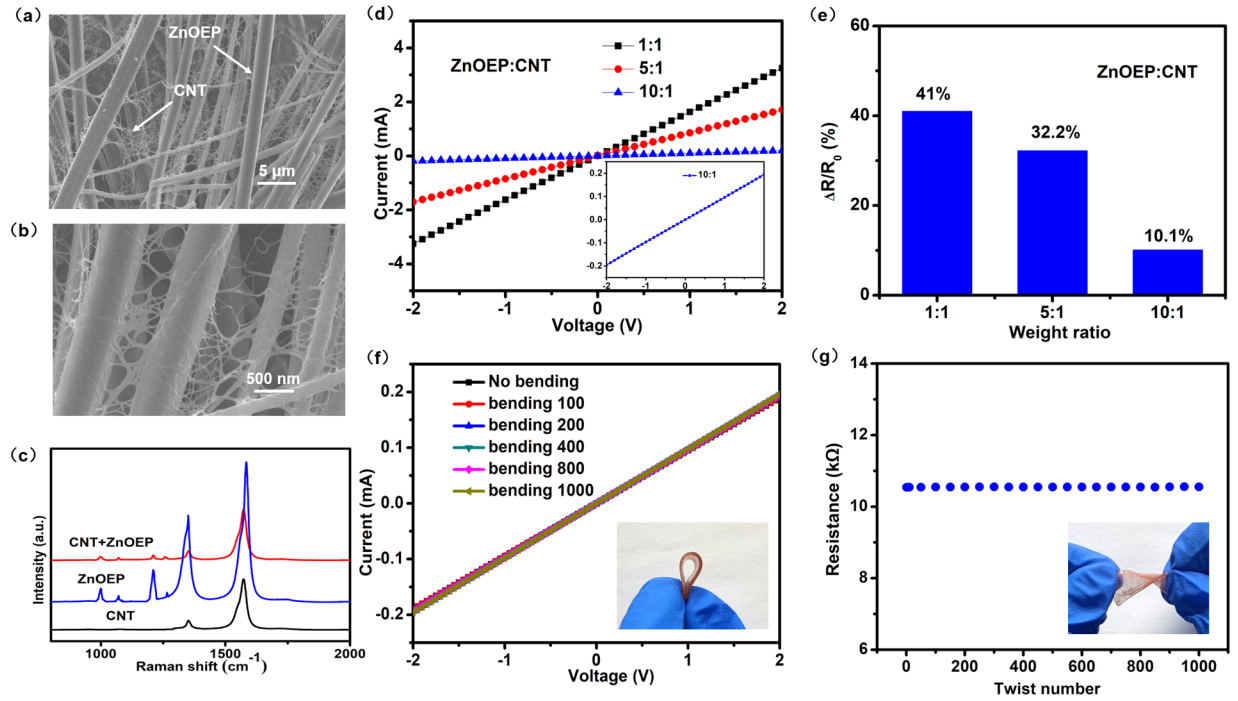

Figure 2. (a) SEM image of the entwined ZnOEP/CNT hybrid network with hierarchical formation of CNTs on ZnOEP. (b) SEM image of dense CNT networks cladded on ZnOEP. (c) Raman spectra of pure ZnOEP, pure CNT, and the ZnOEP/CNT hybrid. (d) Measured $I-V$ curve of the ZnOEP/CNT hybrid with different ZnOEP to CNT mix ratios. (e) Resistance variation of the ZnOEP/CNT hybrid with different ZnOEP to CNT mix ratios under a 90° bending angle. (f) $I-V$ curve of a 10:1 ZnOEP to CNT mixed hybrid under different cycles of bending and recovery test. (g) Resistance of the 10:1 ZnOEP to CNT mixed hybrid under different cycles of twisting and recovery tests.

cobweb-like structure on a micropost array, as illustrated in Figure 1c,d. The hybrid sensing materials float around the micropost, allowing for free and larger deformation of the sensing material compared to the micropost under pressure loading. As a result, the sensitivity, response time, and dynamic range of our sensor are significantly improved. In addition, the self-assembled ZnOEP/CNT hybrid in the form of a cobweb strongly adheres to the top surface of the PDMS posts due to the ZnOEP matrix's low Young's modulus and nonpolar bonding force, as indicated in Figure 1e.

In this work, the fabricated pressure sensor achieves an ultrahigh sensitivity of 39.4 kPa^{-1} from a 10 Pa to 1.6 kPa pressure range, a fast response time of 3 ms, a low detection limit of 10 Pa, and a high stability of over 5000 repeated loading cycles. Also, no delamination or degradation in the resistance was observed after thousand cycles of bending and twisting tests. We demonstrate the application of the flexible pressure sensor as a sensitive e-skin for physiological monitoring, voice recognition, and mechanical vibration detection.

2. EXPERIMENTAL SECTION

2.1. Materials. Carboxylated single-wall CNTs were purchased from XianFeng Nanao Co. Nanjing, China. Chloroform, octane, and propylene glycol methyl ether acetate (PGMEA) were purchased from Aladdin Chemical Co., Shanghai, China. ZnOEP was purchased from Sigma-Aldrich Chemical Co., Ltd. and used without purification. Polydimethylsiloxane (PDMS; Sylgard 184) was purchased from Dow Corning, America.

2.2. Fabrication of Micropost Array. The PDMS micropost arrays were replicated from a silicon mold structured using a photolithography process, which guarantees the consistency of the demolded PDMS substrate each time and saves time for batch fabrication of the pressure sensor. An SU-8 2015 photoresist was spin-coated on a 4 in. silicon wafer at 3000 rpm followed by soft baking at 65 °C for 1 min and 90 °C for 3 min. Then, under UV exposure for 8 s, post-exposure bake was performed at 65 °C for 1 min and 90 °C for 3 min. After developing for 8 s, the template was hard-baked at 150 °C for 30 min. Finally, a mold containing a number of 1 cm × 1 cm arrays of 15 μm deep holes with two different diameters of 30 and 60 μm was obtained. With the design of three smaller posts surrounding each larger post, we aim to enhance the structural integrity of the cobweb-like network during the dip-coating process.Vapor-phase trichloro-(1*H*,1*H*,2*H*,2*H*-perfluorooctyl)silane (FOTS) was subsequently deposited on the mold by thermal evaporation, forming an antisticking monolayer on its surface. Following this, a PDMS elastomer was prepared in a 10:1 weight mix ratio of a base-to-curing agent, casted on the micropatterned mold, and baked in an oven at 80 °C for 4 h. The completed substrate with micropost arrays was finally obtained by peeling off the PDMS from the silicon mold, and ready for coating with the piezoresistive material. The detailed fabrication process is summarized in Figure S1 of the Supporting Information.

2.3. Preparation of ZnOEP/CNT Hybrid and Fabrication of Pressure Sensor. To prepare the hybrid material, a 0.05 mg/mL carboxylated single-wall CNT was first dispersed in chloroform. A 0.5 mg/mL concentration of ZnOEP powder was then dissolved in the CNT solution, yielding a 10:1 weight ratio of ZnOEP to CNT. Octane and PGMEA were subsequently added to the solution to control the rate of evaporation during the self-assembly process in a 2:1:1 volume ratio of chloroform, octane, and PGMEA. The formation of the hybrid material is driven by the conjugated π-bonds of ZnOEP, which have a good affinity for the CNTs as a result of strong noncovalent interactions (i.e., $\pi-\pi$ and van der Waals). The optical photographs of the prepared pure CNT solution, pure ZnOEP solution, and the CNT/ZnOEP mixture are displayed in Figure S2. These images highlight the successful combination of ZnOEP and CNT in solution: black uniformly distributing particles in the red solution can be observed from the mixture in contrast to the pure CNT solution that is completely black and the pure ZnOEP solution that is completely red. With a prepared ZnOEP/CNT hybrid solution, the pressure sensor was fabricated by simply dip-coating the solution on PDMS micropost arrays, as illustrated in Figure S3. Here, the PDMS was mounted on a

https://dx.doi.org/10.1021/acsami.0c12369
ACS Appl. Mater. Interfaces 2020, 12, 48938−48947

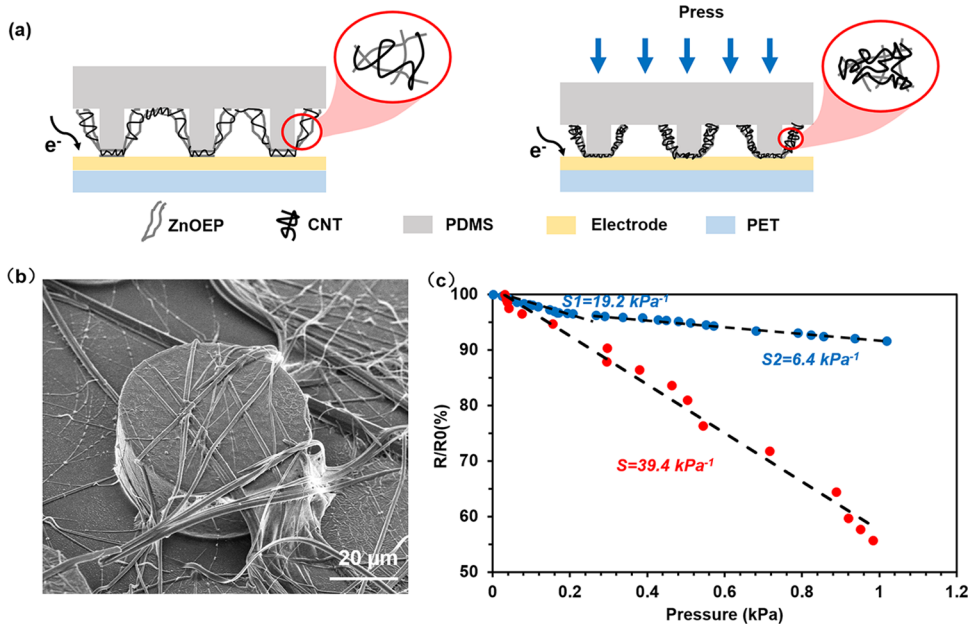

Figure 3. (a) Schematic drawing of the working mechanism of the proposed flexible piezoresistive pressure sensor. (b) SEM image of the ZnOEP/CNT network hanging around the micropost with an enlarged inset showing the hybrid network overhanging the micropost from top to bottom. (c) Comparative study on sensitivity of the pressure sensor with/without micropost arrays under a small pressure range (0−1 kPa).

clean O_2 plasma-treated glass slide to prevent it from rolling up during the ZnOEP/CNT hybrid's self-assembly. This process was completed with solvent evaporation after which the cobweb-like material was formed and grew on the PDMS surface that overspread the entire micropost arrays, as illustrated in Figure S4.

2.4. Characterization of Pressure Sensor. The flexible pressure sensor's performance was characterized using a dynamic fatigue testing system (ElectroPuls 1000, Instron). Here, we applied controllable dynamic and static pressure to the sensor through a customized acrylic cubic probe (1 cm^2 in area) clamped on the upper gripper of the instrument. The resistance of the pressure sensor was measured in real time with a digital multimeter (Agilent 3665A), while its current−voltage (I−V) curves after cycles of bending were measured with a source meter (Keithley 2400). The resistivity of the conductive ZnOEP/CNT network was measured with the same source meter in a four-point probe configuration. The molecular structure of the hybrid material was determined using Raman spectroscopy, performed with an Horiba LabRam HR Evolution tool at a 514 nm wavelength, while the morphology of the ZnOEP/CNT hybrid on the PDMS micropost array was observed by field-emission scanning electron microscopy (FE-SEM; Hitachi SU8010).

3. RESULTS AND DISCUSSION

Figure 2a shows an SEM image of the ZnOEP/CNT hybrid depicting two different network structures of one-dimensional nano/micromaterials entwined together. Larger networks were observed with ZnOEP owing to the strong π−π interaction between ZnOEP molecules, and the result is consistent with previous reported works of ZnOEP networks prepared from solution.[28] The image in Figure 2b shows that CNT not only cladded ZnOEP but also formed denser networks between the ZnOEP framework. This is crucial to the high sensitivity of the sensor as the hierarchical structure formed by suspending nanoscale CNTs on microscale ZnOEPs has previously been proven to be ultrasensitive to external pressure.[42] For a more detailed study of the hybridization process, the molecular composition of the ZnOEP/CNT material was analyzed through Raman spectroscopy. The measured spectra of the ZnOEP/CNT hybrid in comparison with ZnOPE and CNT are depicted in Figure 2c. Here, all the peaks relating to pure ZnOEP and CNT have been merged, indicating complete hybridization of ZnOEP and CNT. The electrical property of the material also supports this hybridization phenomenon. As previously reported, pure ZnOEP exhibits an extremely large resistivity,[41] while CNTs have a large conductivity that dictates the conductivity of the hybrid material. As a result of hybridization, the sheet resistance of the ZnOEP/CNT is about 10^8 times smaller than the resistance of pure ZnOEP but 100 times larger than the resistance of pure CNT, as demonstrated in Figure S5. Concentration of CNT that determines both the electrical and mechanical property of the hybrid material was then examined. I−V curves for ZnOEP/CNT uniformly dip-coated on a flat 1 cm × 4 cm PDMS surface are shown in Figure 2d. Decreasing the concentration of CNT in solution from 50 (i.e., a 1:1 weight ratio of ZnOEP to CNT) to about 9% (10:1 ZnOEP to CNT) decreased the slope of the I−V curve that increased the sheet resistance of the material from 156 to 2566 Ω/□. However, while a larger CNT concentration improves some of the electrical properties of the material, it weakens its mechanical performance; as CNT has a much larger Young's modulus than organic materials like small conjugated molecules,[43,44] a higher concentration of CNT leads to a larger modulus mismatch during the hybridization that is easy to crack. In addition, the increased presence of CNTs would clad the ZnOEP framework that weakens adhesion of the hybrid material to PDMS. It is highlighted with the results of experiments evaluating electrical stability in terms of the variation of resistance under bending conditions, as shown in Figure 2e. With a 50% CNT concentration, there is a 52% variation in resistance at a 90° bending angle. Conversely, there is only a 10% variation in resistance at the same bending angle with a 9% CNT concentration. Hence, in this work, we fabricated the hybrid material using a 9% CNT concentration for balanced electrical and mechanical performance.

A combination of ZnOEP's low Young's modulus, nonpolar bonding between ZnOEP and PDMS, and the increased contact

https://dx.doi.org/10.1021/acsami.0c12369
ACS Appl. Mater. Interfaces 2020, 12, 48938−48947

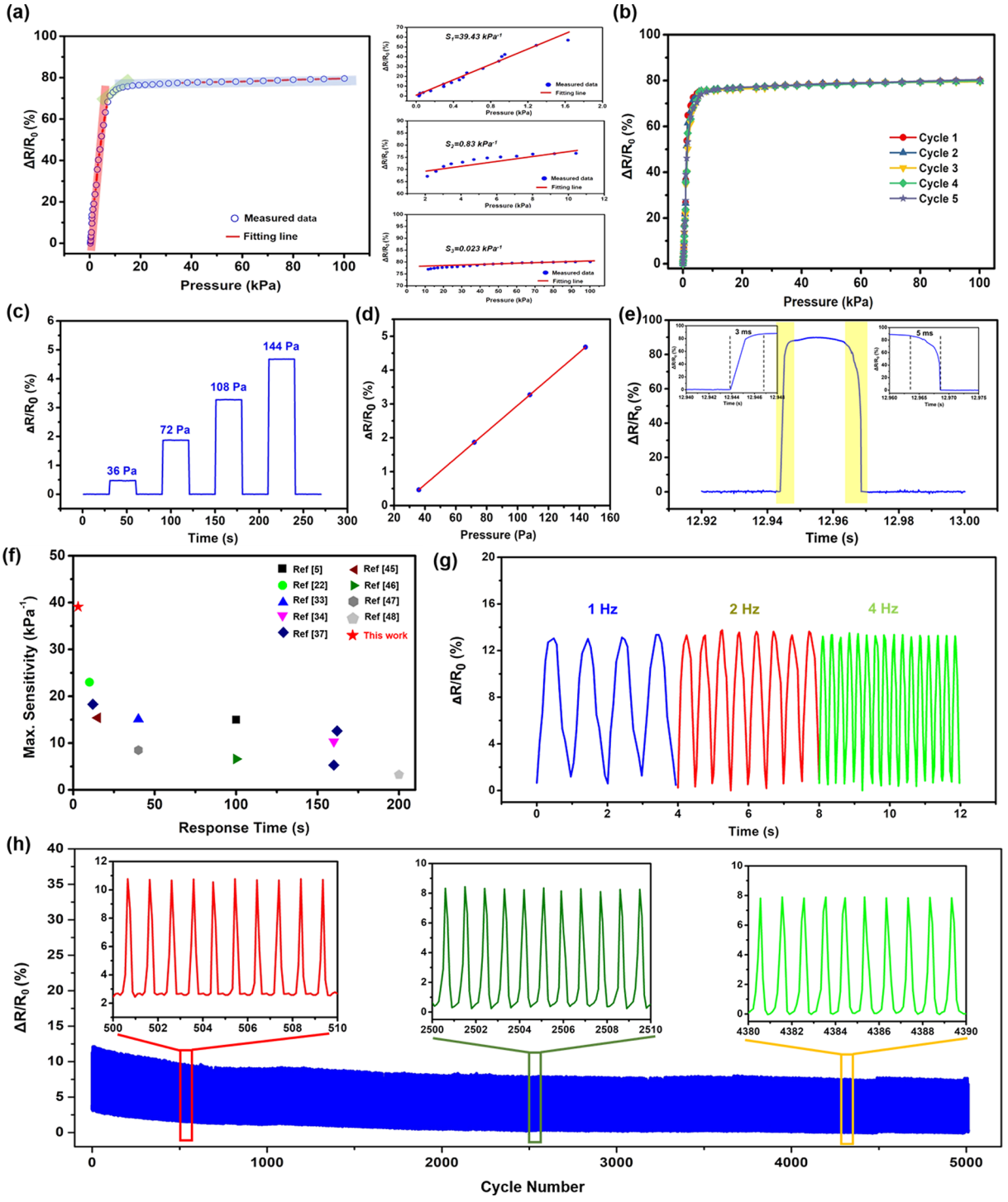

Figure 4. (a) Sensitivity of the flexible pressure sensor with enlarged insertion shows the sensitivity under low (0−1.6 kPa), medium (1.6−10 kPa), and high (10−100 kPa) pressure ranges. (b) Response curve of the sensor after five cycles of repeating the compression test with a pressure from 0 to 100 kPa. (c) Dynamic measurement of the sensor response with an increased pressure from 36 to 144 Pa and (d) linear plotting of the extracted data. (e) Measured response time of the sensor under an applied pressure of 2 kPa with insets showing the response and relaxation time. (f) Comparison of piezoresistive pressure sensors with different microstructures (microdome, micropyramid, and micropillar). (g) Frequency response of the sensor under 340 Pa loading at 1,2, and 4 Hz. (h) Resistance variation of the sensor under 5000 loading/unloading cycles with a pressure of about 250 Pa. Insets demonstrate the enlarged variation at the beginning, middle, and end of the test cycles.

area owing to the microstructured PDMS surface should produce a piezoresistive network with good adhesion to the PDMS substrate. To evaluate the stability of this adhesion, we obtained $I-V$ curves of the piezoresistive network after 1000 cycles of bending and recovery tests, as shown in Figure 2f. Also, twisting and recovery tests of the piezoresistive network were performed where the resistance of 1000 cycles is shown in Figure 2g. After 1000 cycles of bending and twisting, both $I-V$ curves overlapped with the initial value and the resistance remains consistent, showing the stable adhesion of the ZnOEP/CNT

https://dx.doi.org/10.1021/acsami.0c12369
ACS Appl. Mater. Interfaces 2020, 12, 48938−48947

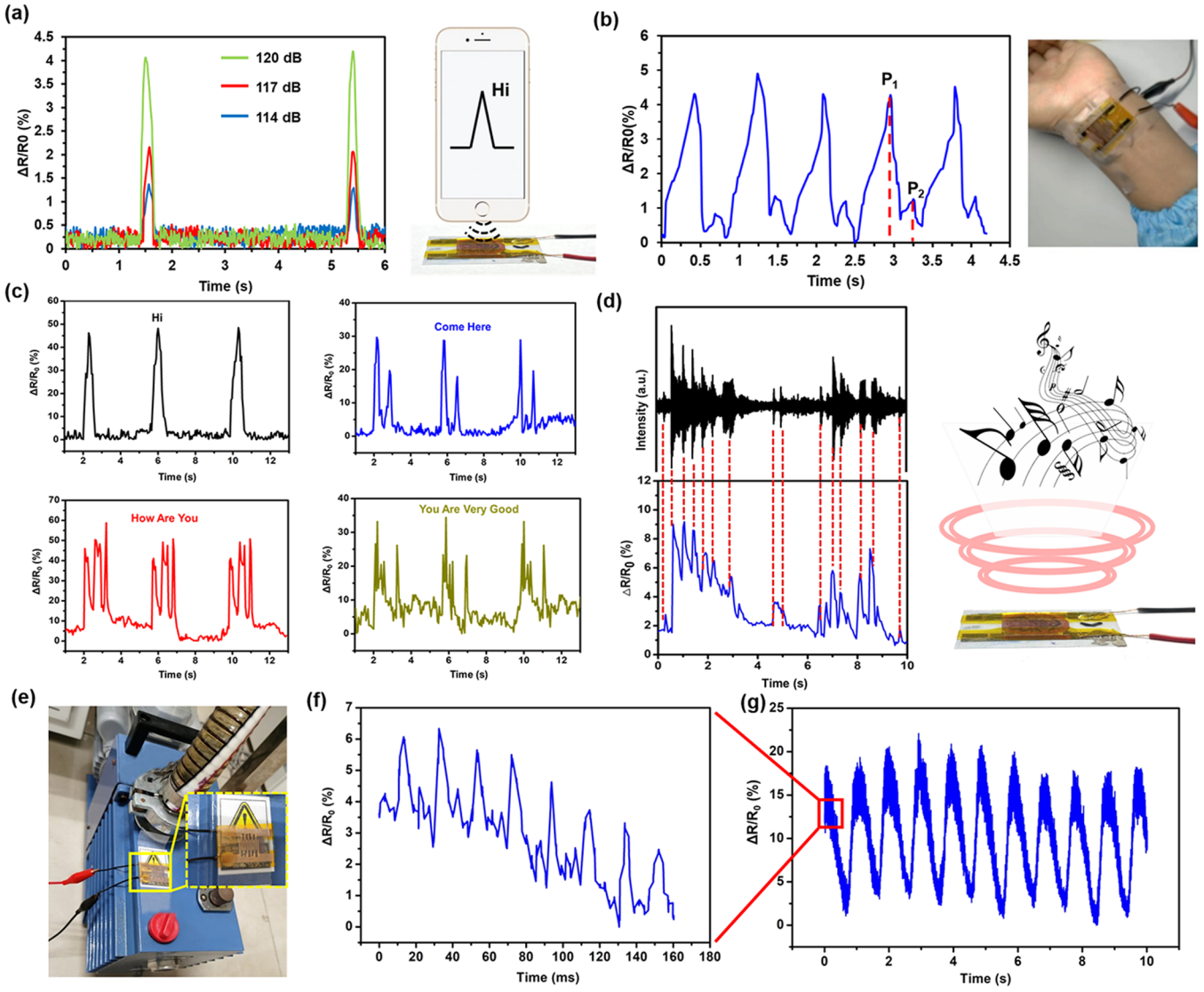

Figure 5. (a) Pressure sensor can be applied to detect the sound pressure level (SPL) by using a cell phone as the sound source. The minimal detectable SPL of the sensor is 114 dB. (b) Sensor is attached to the wrist of a female volunteer and is used to detect the radial artery pulse in which the systolic peak (P1) and diastolic peak (P2) of the blood pressure can be identified. (c) Voice recognition by speaking to the pressure sensor. Real-time distinguishment of short words and phrases like "Hi", "Come Here", "How Are You", and "You Are Very Good" is realized. (d) Acoustic spectrum of a light music and sensor response curve matches well, showing that the pressure sensor can also recognize the rhythm of music. (e) Pressure sensor on the surface of mechanical pump. Mixed vibration spectrum of the (f) high (53 Hz) and (g) low (1 Hz) frequency of the mechanical pump.

hybrid to PDMS. Here, all series measurements distributed around the initial resistance were obtained prior to bending or twisting, proving the stable electrical and mechanical performance of the piezoresistive network.

The working principle of the proposed piezoresistive sensor is dictated by a change in contact resistance in response to loading pressure. As indicated in the schematic drawing of Figure 3a, the hybrid material was constructed in the form of a cobweb-like network and overhung around each individual micropost. Initially, the conductive hybrid material is under a loose condition when no pressure is exerted. Applying external pressure leads to a compression of the cobweb-like network, making the conductive paths closer and denser, as illustrated in the insets of Figure 3a, where more CNTs contact with each other, resulting in a decrease of the resistance of the device. Moreover, the specifically designed micropost structure enables the suspension of the hybrid material around each post and produces overhanging morphology from the top to the bottom surface of the substrate, as shown in Figure 3b. This 3D overhanging cobweb-like structure exhibits two anchored ends and a floating center such that the effective spring constant of the entire structure is smaller compared to the one with a conformal morphology. So, the pressure sensor is more sensitive to external stresses, in general, and tiny stresses, in particular. To verify this effect, we conducted a comparative study on the responses of a planar substrate and the microposted substrate. The change in resistance as a function of external pressures within the range from 0 to 1 kPa for both types of sensors is shown in Figure 3c. Here, we note a 2-fold enhancement in sensitivity using the overhanging morphology on the microstructured substrate compared to the conformal morphology of the hybrid material on a planar substrate.

For a more comprehensive characterization of the pressure sensor, we measured the change in resistance with the applied pressure increasing from 0 to 100 kPa, as shown in Figure 4a. The resulting response curve was divided into three segments of

https://dx.doi.org/10.1021/acsami.0c12369
ACS Appl. Mater. Interfaces 2020, 12, 48938−48947

different sensitivities. As the enlarged views of Figure 4a show that the sensor's response is linear in each segment, we calculated this sensitivity as

$$S = (\Delta R/R_0)/\Delta P \quad (1)$$

where $(\Delta R/R_0)$ is the fractional change in resistance and P is the applied pressure. Hence, we obtained an ultrahigh sensitivity of about 39.4 kPa^{-1} in the 0−1.6 kPa range (low pressure), a reduced sensitivity of 0.83 kPa^{-1} in the 1.6−10 kPa range (medium pressure), and a minimal sensitivity of 0.023 kPa^{-1} in the high pressure range (10−100 kPa). As explained above, the sensor's ultrahigh sensitivity is a result of using a network-structured material with overhanging morphology. For pressures higher than 1.6 kPa, the sensor's response is dictated by the compression of the microposts together with the hybrid material. At this point, these posts work as a series of springs with different spring constants in parallel. The effective spring constant of this system is much larger than the overhanging hybrid material, leading to a drop in the sensitivity. Similarly, for pressures higher than 10 kPa, both the hybrid material and the micropost arrays are saturated, and the sensor's response is determined by the compression of a flexible substrate. As the effective spring constant of the whole device is much larger, it corresponds to the significant drop in sensitivity. Further improvement of sensitivity and pressure sensing range can be achieved through designing a more compressible substrate. For example, using a lower curing agent-to-base solution ratio can decrease the stiffness of the PDMS microposts, which is helpful to improve the dynamic measurement range of the pressure sensor. In addition, we can introduce microposts with more height difference. When higher microposts are compressed to a certain distance, lower ones will start to bear the load and the cobweb-like sensing network on the lower microposts can detect the extra pressure. With more groups of microposts of different heights, the sensor can sustain larger pressure loading.

The repeatability of the sensor was evaluated by measuring its response under five cycles of compression test with a pressure from 0 to 100 kPa. The response curves in Figure 4b overlapped with each other, indicating a stable sensing performance and repeatability in low, medium, and high pressure ranges. The real-time dynamic response of the sensor was examined by applying an increased loading pressure from 36 to 144 Pa, as shown in Figure 4c. Notably from Figure 4c, with a fixed increasing pressure interval of 36 Pa, the sensor exhibited good linearity as the extraction data plotted in Figure 4d. The sensor also exhibited a fast response to external stress as a further benefit of the overhanging cobweb-like hybrid material that the dense CNT conducting network can rapidly response to the external stimuli and lead to the change of resistance. The insets in Figure 4e indicate an ultrafast response and relaxation time of 3 and 5 ms, respectively, for a given 2 kPa loading pressure. Benefitting from the bioinspired 3D cobweb-like structure, both the sensitivity and response time of the proposed sensor are superior than previously reported piezoresistive pressure sensors with similar microstructure designs, including the microdome, micropyramid, and micropillar,[5,22,33,34,37,45−48] as shown in Figure 4f. The frequency response of the pressure is also characterized in Figure 4g. Under 340 Pa loading applied at 1, 2, and 4 Hz, the sensor responded accurately and stably to corresponding frequencies. Finally, to evaluate the long-term stability of the fabricated sensor, a repetitive loading/unloading dynamic test was performed at a frequency of 1 Hz. The relative change in resistance remained practically constant after 5000 cycles of testing, as shown in Figure 4h, proving the high stability of the sensor with respect to long-term use. Similarly, the change in resistance at the beginning and end of the test cycles are virtually the same, as shown in the insets, further implying the good reliability and repeatability of the pressure sensor.

To evaluate the detect limitation of the proposed pressure sensor, sound pressure was measured by fixing the sensor close to the loudspeaker of a cell phone (Figure 5a). The sound pressure level (SPL) that was measured using a sound meter gradually decreased from 120 dB by varying the volume of cell phone. The exact sound pressure P was calculated as

$$P = P_0 \times 10^{(\mathrm{SPL}/20)} \quad (2)$$

where P_0 is the reference pressure (2×10^{-5} Pa). So, it could be used to characterize the dynamic response of the sensor. The change in resistance decreased as the SPL decreased, and finally, a detection limit of 10 Pa (114 dB) was obtained. Benefitting from the ultrahigh sensitivity and fast response of the pressure sensor, it can also be used for detection of physiological signals. As a demonstration, the sensor was attached on the wrist of a volunteer to measure the radial artery pulse. A periodic variation in the sensor's resistance, reflecting the volunteer's wrist pulse wave, is shown in Figure 5b. The systolic peak and diastolic peak of the blood pressure (labeled as P1 and P2, respectively) can clearly be distinguished from this waveform. The sensor can also be used for voice recognition, with words and phrases being distinguished as a characteristic resistance pattern output by the sensor. For instance, the peaks in Figure 5c represent the syllables produced in pronunciation of simple words and phrases like "Hi", "Come Here", "How Are You", and "You Are Very Good" were spoken directly to the pressure sensor. Moreover, with the rapid response, the sensor could also recognize fast rhythms from light music, as shown in Figure 5d (a video of this test is included as Movie S1 in the Supporting Information). It can be noted that the response curve of the sensor at the bottom of the figure matches well with the acoustic spectrum of the music depicted in the upper part of the figure. The ultrafast response of the sensor can also be applied in the industrial field for vibration detection, such as mechanical pump vibration monitoring. By attaching the flexible pressure sensor on the pump surface, as shown in Figure 5e, the mechanical vibration induced by the motor can be directly measured. The vibrating frequency of the pump that reflects its healthy operation condition is a complicated and mixed spectrum from low to high frequencies. The high frequency is from the rotation of a driving motor, and the low frequency is from the motor-induced vibration of supporting structures, and as shown in Figure 5f,g, both high (53 Hz) and low (1 Hz) frequencies can be clearly distinguished by the sensor. These results indicate that our pressure sensor can be employed for diver applications, including voice recognition, physiological detection, and mechanical vibration monitoring owing to its ultrahigh sensitivity and fast response.

4. CONCLUSIONS

In this study, we developed a resistive pressure sensor with an ultrahigh sensitivity, rapid response, and low detection limit based on an organic/inorganic hybrid material dip-coated on a PDMS substrate with micropost arrays. Inspired by the cobweb in nature, a cobweb-like composite structure made of ZnOEP and CNTs material was proposed as a piezoresistive network with good flexibility and conductivity. Coupled with its

https://dx.doi.org/10.1021/acsami.0c12369
ACS Appl. Mater. Interfaces 2020, 12, 48938−48947

suspension around the microposts to form an overhanging morphology, the free deformable 3D network of the material resulted in an ultrahigh sensitivity (39.4 kPa^{-1} up to 1.6 kPa) and fast response time (3 ms). In addition, the nonpolar force between ZnOEP and PDMS and the increased contact area between the cobweb-like network material and the microstructured PDMS surface improved the bonding of the material to the flexible substrate so that, after 1000 cycles of bending and twisting tests, it remained firmly attached to the PDMS. In addition, the pressure sensor's performance remained stable and reliable over 5000 cycles of the loading/unloading test. We were consequently able to demonstrate the use of our sensor in diverse applications, including sound level measurement, wrist pulse monitoring, voice recognition for both speech and music, and mechanical vibration monitoring, suggesting that the proposed flexible pressure sensor can be applied in fields like healthcare monitoring, soft robotics sensing, and human–machine interface.

■ ASSOCIATED CONTENT

Supporting Information

The Supporting Information is available free of charge at https://pubs.acs.org/doi/10.1021/acsami.0c12369.

Fabrication process of the PDMS substrate with a micropost array; optical photograph of ZnOEP, CNT, and ZnOEP/CNT hybridized solution; the fabrication process of the flexible pressure sensor with a cobweb-like hybrid on a micropost array; optical and SEM images of the cobweb-like hybrid material; and the $I-V$ curves of pure ZnOEP, CNT, and the ZnOEP/CNT hybrid (PDF)

Application of the sensor for the rhythm detection of light music (MP4)

■ AUTHOR INFORMATION

Corresponding Authors

Zhengchun Peng − *Guangdong Provincial Key Laboratory of Micro/Nano Optomechatronic Engineering, College of Mechatronics and Control Engineering and Key Laboratory of Optoelectronic Devices and Systems of Ministry of Education and Guangdong Province, College of Physics and Optoelectronic Engineering, Shenzhen University, Shenzhen 518060, China;* orcid.org/0000-0002-7114-1797; Email: zcpeng@szu.edu.cn

Hao Wang − *Guangdong Provincial Key Laboratory of Micro/Nano Optomechatronic Engineering, College of Mechatronics and Control Engineering, Shenzhen University, Shenzhen 518060, China;* orcid.org/0000-0001-8896-5496; Email: whao@szu.edu.cn

Authors

Weiguan Zhang − *Guangdong Provincial Key Laboratory of Micro/Nano Optomechatronic Engineering, College of Mechatronics and Control Engineering and Key Laboratory of Optoelectronic Devices and Systems of Ministry of Education and Guangdong Province, College of Physics and Optoelectronic Engineering, Shenzhen University, Shenzhen 518060, China*

Yan Xiao − *Key Laboratory of Optoelectronic Devices and Systems of Ministry of Education and Guangdong Province, College of Physics and Optoelectronic Engineering, Shenzhen University, Shenzhen 518060, China*

Yu Duan − *Key Laboratory of Optoelectronic Devices and Systems of Ministry of Education and Guangdong Province, College of Physics and Optoelectronic Engineering, Shenzhen University, Shenzhen 518060, China*

Ning Li − *Key Laboratory of Optoelectronic Devices and Systems of Ministry of Education and Guangdong Province, College of Physics and Optoelectronic Engineering, Shenzhen University, Shenzhen 518060, China*

Linlin Wu − *Key Laboratory of Optoelectronic Devices and Systems of Ministry of Education and Guangdong Province, College of Physics and Optoelectronic Engineering, Shenzhen University, Shenzhen 518060, China*

Yan Lou − *Guangdong Provincial Key Laboratory of Micro/Nano Optomechatronic Engineering, College of Mechatronics and Control Engineering, Shenzhen University, Shenzhen 518060, China*

Complete contact information is available at: https://pubs.acs.org/10.1021/acsami.0c12369

Author Contributions

W.Z. designed, fabricated, and characterized the device and wrote the manuscript. Y.X. prepared and characterized the conductive small organic molecules. N.L., Y.D., L.W., and Y.L. assisted with the application of the device and the demonstrations. H.W. and Z.P. provided regular guidance to the research and revised the manuscript. Z.P. and W.Z. conceived the original idea. All authors discussed the results and commented on the manuscript.

Notes

The authors declare no competing financial interest.

■ ACKNOWLEDGMENTS

This work was financially supported by the Shenzhen Science and Technology Program (JCYJ20190808142609414, KQTD20170810105439418, JCYJ20170817094728456, and JCYJ20170818091233245), the National Natural Science Foundation of China (61904112, 51675347, 61671308, and 61903259), the Postdoctoral Science Foundation of China (2019 M650209), the National Key R&D Program of China (2019YFB2204500), and the Department of Education of Guangdong Province (2016KZDXM005).

■ REFERENCES

(1) Gorissen, B.; Reynaerts, D.; Konishi, S.; Yoshida, K.; Kim, J. W.; De Volder, M. Elastic Inflatable Actuators for Soft Robotic Applications. *Adv. Mater.* **2017**, *29*, 1604977.

(2) Gao, Y.; Yu, L.; Yeo, J. C.; Lim, C. T. Flexible Hybrid Sensors for Health Monitoring: Materials and Mechanisms to Render Wearability. *Adv. Mater.* **2019**, *32*, 1902133.

(3) Guo, Y.; Guo, Z.; Zhong, M.; Wan, P.; Zhang, W.; Zhang, L. A Flexible Wearable Pressure Sensor with Bioinspired Microcrack and Interlocking for Full-Range Human-Machine Interfacing. *Small* **2018**, *14*, 1803018.

(4) Park, H.; Jeong, Y. R.; Yun, J.; Hong, S. Y.; Jin, S.; Lee, S.-J.; Zi, G.; Ha, J. S. Stretchable Array of Highly Sensitive Pressure Sensors Consisting of Polyaniline Nanofibers and Au-coated Polydimethylsiloxane Micropillars. *ACS Nano* **2015**, *9*, 9974−9985.

(5) Zhang, Y.; Hu, Y.; Zhu, P.; Han, F.; Zhu, Y.; Sun, R.; Wong, C.-P. Flexible and Highly Sensitive Pressure Sensor Based on Microdome-Patterned PDMS Forming with Assistance of Colloid Self-Assembly and Replica Technique for Wearable Electronics. *ACS Appl. Mater. Interfaces* **2017**, *9*, 35968−35976.

(6) Shao, Q.; Niu, Z.; Hirtz, M.; Jiang, L.; Liu, Y.; Wang, Z.; Chen, X. High-Performance and Tailorable Pressure Sensor Based on Ultrathin Conductive Polymer Film. *Small* **2014**, *10*, 1466−1472.

(7) Yoon, S. G.; Park, B. J.; Chang, S. T. Highly Sensitive Piezocapacitive Sensor for Detecting Static and Dynamic Pressure Using Ion-Gel Thin Films and Conductive Elastomeric Composites. *ACS Appl. Mater. Interfaces* **2017**, *9*, 36206−36219.
(8) Yang, J.; Luo, S.; Zhou, X.; Li, J.; Fu, J.; Yang, W.; Wei, D. Flexible, Tunable, and Ultrasensitive Capacitive Pressure Sensor with Microconformal Graphene Electrodes. *ACS Appl. Mater. Interfaces* **2019**, *11*, 14997−15006.
(9) Chen, Z.; Wang, Z.; Li, X.; Lin, Y.; Luo, N.; Long, M.; Zhao, N.; Xu, J.-B. Flexible Piezoelectric-Induced Pressure Sensors for Static Measurements Based on Nanowires/Graphene Heterostructures. *ACS Nano* **2017**, *11*, 4507−4513.
(10) Park, D. Y.; Joe, D. J.; Kim, D. H.; Park, H.; Han, J. H.; Jeong, C. K.; Park, H.; Park, J. G.; Joung, B.; Lee, K. J. Self-Powered Real-Time Arterial Pulse Monitoring Using Ultrathin Epidermal Piezoelectric Sensors. *Adv. Mater.* **2017**, *29*, 1702308.
(11) Chun, J.; Lee, K. Y.; Kang, C.-Y.; Kim, M. W.; Kim, S.-W.; Baik, J. M. Embossed Hollow Hemisphere-Based Piezoelectric Nanogenerator and Highly Responsive Pressure Sensor. *Adv. Funct. Mater.* **2014**, *24*, 2038−2043.
(12) Garcia, C.; Trendafilova, I.; De Villoria, R. G.; del Rio, J. S. Self-Powered Pressure Sensor Based on the Triboelectric Effect and Its Analysis Using Dynamic Mechanical Analysis. *Nano Energy* **2018**, *50*, 401−409.
(13) Lee, K. Y.; Yoon, H.-J.; Jiang, T.; Wen, X.; Seung, W.; Kim, S.-W.; Wang, Z. L. Fully Packaged Self-Powered Triboelectric Pressure Sensor Using Hemispheres-Array. *Adv. Energy Mater.* **2016**, *6*, 1502566.
(14) Ha, M.; Park, J.; Lee, Y.; Ko, H. Triboelectric Generators and Sensors for Self-Powered Wearable Electrics. *ACS Nano* **2015**, *9*, 3421−3427.
(15) Li, B.; Gil, B.; Power, M.; Gao, A.; Treratanakulchai, S.; Anastasova, S.; Yang, G.-Z. Garbon-Nanotube-Coated 3D Microspring Force Sensor for Medical Applications. *ACS Appl. Mater. Interfaces* **2019**, *11*, 35577−35586.
(16) Chun, S.; Son, W.; Choi, C. Flexible Pressure Sensors Using Highly-Oriented and Free-Standing Carbon Nanotube Sheets. *Carbon* **2018**, *139*, 586−592.
(17) Xia, K.; Wang, C.; Jian, M.; Wang, Q.; Zhang, Y. CVD Growth of Fingerprint-Like Patterned 3D Graphene Film for an Ultrasensitive Pressure Sensor. *Nano Res.* **2018**, *11*, 1124−1134.
(18) Xing, C.; Jing, G.; Liang, X.; Qiu, M.; Li, Z.; Cao, R.; Li, X.; Fan, D.; Zhang, H. Graphene Oxide/Black Phosphorus Nanoflake Aerogels with Robust Thermal-Stability and Significantly Enhanced Photothermal Properties in Air. *Nanoscale* **2017**, *9*, 8096.
(19) Wei, Y.; Chen, S.; Lin, Y.; Yuan, X.; Liu, L. Silver Nanowires Coated on Cotton for Flexible Pressure Sensors. *J. Mater. Chem. C* **2016**, *4*, 935−943.
(20) Jo, H. S.; An, S.; Park, C.-W.; Woo, D.-Y.; Yarin, A. L.; Yoon, S. S. Wearable, Stretchable, Transparent All-in-One Soft Sensor Formed from Supersonically Sprayed Silver Nanowires. *ACS Appl. Mater. Interfaces* **2019**, *11*, 40232−40242.
(21) Gong, S.; Schwalb, W.; Wang, Y.; Chen, Y.; Tang, Y.; Si, J.; Shirinzadeh, B.; Cheng, W. A Wearable and Highly Sensitive Pressure Sensor with Ultrathin Gold Nanowires. *Nat. Commun.* **2014**, *5*, 3132.
(22) Zhu, B.; Ling, Y.; Yap, L. W.; Yang, M.; Lin, F.; Gong, S.; Wang, Y.; An, T.; Zhao, Y.; Cheng, W. Hierarchically Structured Vertical Gold Nanowire Array-Based Wearable Pressure Sensors for Wireless Health Monitoring. *ACS Appl. Mater. Interfaces* **2019**, *11*, 29014−29021.
(23) Gaynor, W.; Burkhard, G. F.; McGehee, M. D.; Peumans, P. Smooth Nanowire/Polymer Composite Transparent Electrodes. *Adv. Mater.* **2011**, *23*, 2905−2910.
(24) Li, Y.; Cui, P.; Wang, L.; Lee, H.; Lee, K.; Lee, H. Highly Bendable, Conductive, and Transparent Film by Enhanced Adhesion of Silver Nanowires. *ACS Appl. Mater. Interfaces* **2013**, *5*, 9155−9160.
(25) Ahn, Y.; Jeong, Y.; Lee, Y. Improved Thermal Oxidation Stability of Solution-Processable Silver Nanowire Transparent Electrode by Reduced Graphene Oxide. *ACS Appl. Mater. Interfaces* **2012**, *4*, 6410−6414.
(26) Kim, C.-L.; Jung, C.-W.; Oh, Y.-J.; Kim, D.-E. A Highly Flexible Transparent Conductive Electrode Based on Nanomaterials. *NPG Asia Mater.* **2017**, *9*, No. e438.
(27) Elmoselhy, S. A. M. Hybrid Organic/Inorganic Nano-I-Beam for Structural Nano-mechanics. *Sci. Rep.* **2019**, *9*, 18324.
(28) Park, C.; Park, J. E.; Choi, H. C. Crystallization-Induced Properties from Morphology-Controlled Organic Crystals. *Acc. Chem. Res.* **2014**, *47*, 2353−2364.
(29) Wang, F. X.; Liu, Y. Q.; Wu, H. D.; Xiao, Y.; Pan, G. B. One-Step Fabrication of an Ultralong Zinc Octaethylporphyrin Nanowire Network with High-Performance Photoresponse. *J. Mater. Chem. C* **2013**, *1*, 422−425.
(30) Xu, Y.; Liu, Z.; Zhang, X.; Wang, Y.; Tian, J.; Huang, Y.; Ma, Y.; Zhang, X.; Chen, Y. A Graphene Hybrid Material Covalently Functionalized with Porphyrin: Synthesis and Optical Limiting Property. *Adv. Mater.* **2009**, *21*, 1275−1279.
(31) Shen, D.; Pang, A.; Li, Y.; Dou, J.; Wei, M. Metal-organic frameworks at interfaces of hybrid perovskite solar cells for enhanced photovoltaic properties. *Chem. Commun.* **2018**, *54*, 1253.
(32) Niazov-Elkan, A.; Weissman, H.; Dutta, S.; Cohen, S. R.; Iron, M. A.; Pinkas, I.; Bendikov, T.; Rybtchinski, B. Self-Assembled Hybrid Materials Based on Organic Nanocrystals and Carbon Nanotubes. *Adv. Mater.* **2018**, *30*, 1705027.
(33) Park, J.; Lee, Y.; Hong, J.; Ha, M.; Jung, Y.-D.; Lim, H.; Kim, S. Y.; Ko, H. Giant Tunneling Piezoresistance of Composite Elastomers with Interlocked Microdome Arrays for Ultrasensitive and Multimodal Electronic Skins. *ACS Nano* **2014**, *8*, 4689−4697.
(34) Choong, C. L.; Shim, M. B.; Lee, B. S.; Jeon, S.; Ko, D. S.; Kang, T. H.; Bae, J.; Lee, S. H.; Byun, K. E.; Im, J.; Jeong, Y. J.; Park, C. E.; Park, J. J.; Chung, U. I. Highly Stretchable Resistive Pressure Sensors Using a Conductive Elastomeric Composite on a Micropyramid Array. *Adv. Mater.* **2014**, *26*, 3451−3458.
(35) Shu, Y.; Tian, H.; Yang, Y.; Li, C.; Cui, Y.; Mi, W.; Li, Y.; Wang, Z.; Deng, N.; Peng, B.; Ren, T. L. Surface-Modified Piezoresistive Nanocomposite Flexible Pressure Sensors with High Sensitivity and Wide Linearity. *Nanoscale* **2015**, *7*, 8636−8644.
(36) Luo, Y.; Shao, J.; Chen, S.; Chen, X.; Tian, H.; Li, X.; Wang, L.; Wang, D.; Lu, B. Flexible Capacitive Pressure Sensor Enhanced by Tilted Micropillar Arrays. *ACS Appl. Mater. Interfaces* **2019**, *11*, 17796−17803.
(37) Park, J.; Kim, J.; Hong, J.; Lee, H.; Lee, Y.; Cho, S.; Kim, S.-W.; Kim, J. J.; Kim, S. Y.; Ko, H. Tailoring Force Sensitivity and Selectivity by Microstructure Engineering of Multidirectional Electronic Skins. *NPG Asia Mater.* **2018**, *10*, 163−176.
(38) Shi, J.; Wang, L.; Dai, Z.; Zhao, L.; Du, M.; Li, H.; Fang, Y. Multiscale Hierarchical Design of a Flexible Piezoresistive Pressure Sensor with High Sensitivity and Wide Linearity Range. *Small* **2018**, *14*, 1800819.
(39) Jia, J.; Huang, G.; Deng, J.; Pan, K. Skin-Inspired Flexible and High-Sensitivity Pressure Sensors Based on rGO Films with Continuous-Gradient Wrinkles. *Nanoscale* **2019**, *11*, 4258−4266.
(40) Amoli, V.; Kim, S. Y.; Kim, J. S.; Choi, H.; Koo, J.; Kim, D. H. Biomimetics for High-Performance Flexible Tactile Sensors and Advanced Artificial Sensory Systems. *J. Mater. Chem. C* **2019**, *7*, 14816−14844.
(41) Tang, X.; Wu, C.; Gan, L.; Zhang, T.; Zhou, T.; Huang, J.; Wang, H.; Xie, C.; Zeng, D. Ultrahigh Sensitivity and Ultrawide Pressure Range for Versatile Electronic Skins. *Small* **2019**, *15*, 1804559.
(42) Wang, Z.; Guan, X.; Huang, H.; Wang, H.; Lin, W.; Peng, Z. Full 3D Printing of Stretchable Piezoresistive Sensor with Hierarchical Porosity and Multimodulus Architecture. *Adv. Funct. Mater.* **2019**, *29*, 1807569.
(43) Lau, K. T.; Gu, C.; Hui, D. A Critical Review on Nanotube and Nanotube/Nanoclay Related Polymer Composite Materials. *Compos. Part B-Eng.* **2006**, *37*, 425−436.
(44) Wu, R.; Yan, L.; Zhang, Y.; Ren, J.; Bao, D.; Zhang, H.; Wang, Y.; Du, S.; Huan, Q.; Gao, H.-J. Self-Assembled Patterns and Young's Modulus of Single-Layer Naphthalocyanine Molecules on Ag (111). *J. Phys. Chem. C* **2015**, *119*, 8208−8212.

https://dx.doi.org/10.1021/acsami.0c12369
ACS Appl. Mater. Interfaces 2020, 12, 48938−48947

(45) Li, Z.; Zhang, B.; Li, K.; Zhang, T.; Yang, X. A Wide Linearity Range and High Sensitivity Flexible Pressure Sensor with Hierarchical Microstructures via Laser Marking. *J. Mater. Chem. C* **2020**, *8*, 3088.
(46) Zhang, Y.; Han, F.; Hu, Y.; Xiong, Y.; Gu, H.; Zhang, G.; Zhu, P.; Sun, R.; Wong, C.-P. Flexible and Highly Sensitivity Pressure Sensor with Surface Discrete Microdomes Made from Self-Assembled Polymer Microspheres Array. *Macromol. Chem. Phys.* **2020**, *221*, 2000073.
(47) Cao, Y.; Li, T.; Gu, Y.; Luo, H.; Wang, S.; Zhang, T. Fingerprint-Inspired Flexible Tactile Sensor for Accurately Discerning Surface Texture. *Small* **2018**, *14*, 1703902.
(48) Bae, G. Y.; Pak, S. W.; Kim, D.; Lee, G.; Kim, D. H.; Chung, Y.; Cho, K. Linearly and Highly Pressure-Sensitive Electronic Skin Based on a Bioinspired Hierarchical Structural Array. *Adv. Mater.* **2016**, *28*, 5300−5306.

https://dx.doi.org/10.1021/acsami.0c12369
ACS Appl. Mater. Interfaces 2020, 12, 48938−48947